ASTRONOMY & ASTROPHYSICS
SUPPLEMENT SERIES

Astron. Astrophys. Suppl. Ser. **127,** 497-504 (1998)

Recent developments in superconducting tunnel junctions for ultraviolet, optical & near infrared astronomy

T. Peacock, P. Verhoeve, N. Rando, C. Erd, M. Bavdaz, B.G. Taylor, and D. Perez

Astrophysics Division, Space Science Department of the European Space Agency, ESTEC, PO Box 299,2200 AG Noordwijk, The Netherlands

Received March 20; accepted June 11, 1997

Abstract. Some recent results associated with the development of tantalum based photon counting superconducting tunnel junctions (STJ) suitable for use as broadband low resolution spectrometers for optical and ultraviolet astronomy are presented. A 20×20 μm square tantalum based STJ, operated at a temperature of 0.3 K, has demonstrated a limiting resolution of $\sim$ 8 nm at 200 nm and $\sim$ 80 nm at 1000 nm. The device is extremely linear in response with photon energy, and covers the waveband from 200 nm to 2 μm while measuring the individual photon wavelength and arrival time. The short wavelength limit is currently constrained by the current experimental configuration (a fibre optic) as well as to some extent the sapphire substrate. The estimated quantum efficiency for single photons is over $\sim$ 50% between 200 and 700 nm with a maximum of $\sim$ 75% at 550 nm. Such an STJ when packaged into an array could contribute significantly to many fields of near infrared, optical and ultraviolet astronomy being able to provide efficiently and simultaneously the broad band spectrum and photon arrival time history of every single object in the field over a very wide dynamic range.

Key words: instrumentation: detectors — photometry — superconductors — tunnel junctions — optical/ultraviolet spectroscopy

1. Introduction

A variety of astronomical observations at optical and ultraviolet wavelengths require an efficient detector covering a wide wavelength range from the Lyman limit to the near infrared which can simultaneously provide the wavelength, time of arrival and location of every single photon falling upon the detector from the widest possible field. A detector which possesses the ability to measure the wavelength of individual optical photons has up until now not existed.

A superconductor is theoretically capable of detecting individual optical/UV photons and also measuring the photon energy (Wood & White 1969; Perryman et al. 1993). This ability simply arises from the very small energy gap Δ, of order meV, in a superconductor between the ground state, as represented by the bound Cooper electron pairs, and the first excited state, containing broken Cooper pairs or quasiparticles. The recent experimental demonstration of photon counting at optical wavelengths, coupled to a crude wavelength discrimination with niobium based superconductors (spectral resolution $\Delta\lambda \sim 40$ nm at $\lambda \sim 500$ nm) by Peacock et al. (1996, 1997a)), has clearly shown the validity of this concept. A theoretical evaluation of the limits of $\Delta\lambda$ for various superconductors other than niobium has been made by Peacock et al. (1997b) and supported through recent improved experimental measurements in niobium and tantalum (Peacock et al. 1996c; Verhoeve et al. 1996a).

In this paper we report on measurements from the ultraviolet to the near infrared on a tantalum based superconducting tunnel junction. This is an efficient high speed photon counting detector which has a far improved spectral resolution $\Delta\lambda$ and wavelength coverage compared to the original niobium based device reported by Peacock et al. (1996, 1997a,b). The resolution of this tantalum detector may well provide a contribution in fields as diverse as fast spectro-photometry to deep field imaging. Indeed provided these detectors can be packaged into arrays their existing performance may already be such that they could allow the simultaneous measurement of broad band low resolution spectra of very faint extragalactic sources to be obtained for all objects in the field. Such spectra containing emission line complexes or continuum absorption features (the Lyman edge) in very faint extragalactic objects may allow the direct determination of red shifts.

2. The STJ principle of operation

The absorption of a photon of wavelength λ(nm) in a superconductor is followed by a series of fast processes in which the photon energy is converted into a population of free charge carriers known as quasiparticles in excess of any thermal population. For typical transition metal superconductors this conversion process is of order of a few nanoseconds. At sufficiently low temperatures (typically about an order of magnitude lower than the superconductor's critical temperature T_c) the number density of thermal carriers is very small and the number of excess carriers N_0 created as a result of the absorption of a photon of wavelength λ is inversely proportional to the photon wavelength. In general N_0 can be written:

$$N_0(\lambda) \sim 7\ 10^5/\lambda\Delta(T). \quad (1)$$

Here the wavelength is in nm and the energy gap is in meV. Thus in a Tantalum superconductor at a temperature well below the critical temperature, ($T_c \sim 4.5$ K and $\Delta_{Ta} \sim 0.664$ meV), the initial number of free charge carriers $N_0(\lambda)$ created by the photoabsorption of an optical photon is of order $\sim 2\ 10^3$ for a photon with $\lambda \sim 500$ nm. The fluctuations in the initial number of quasiparticles N_0 depends on the Fano factor F of the superconductor and is the fundamental limit to the spectral resolution (Fano 1947). The Fano limited wavelength resolution in Tantalum is ~ 12 nm at $\lambda \sim 500$ nm. For a full description of the photoabsorption process in a superconductor as well as the spectroscopic capabilities when related to superconducting tunnel junctions the reader is referred to Rando et al. (1992) and Peacock et al. (1997b) respectively.

The quasiparticles produced after photoabsorption in a superconducting thin film can be detected by applying a d.c. potential across two such films separated by a thin insulating barrier; forming a superconducting tunnel junction (STJ). This potential favours the transfer of quasiparticles from one film to the other through quantum-mechanical tunneling across the barrier. The detector signal is therefore represented by the current developed by this tunnel process. After initial tunneling, a quasiparticle can tunnel back, therefore contributing many times to the overall signal (Gray 1978). On average each quasiparticle will contribute $< n >$ times to the signal. Hence the number of effective charge carriers N which appear to have been created is $N =< n > N_0$. Further experimental details of the characteristics associated with this multiple tunneling, which is equivalent to an internal amplification within the junction, can be found in Poelaert et al. (1996).

The initial fluctuation in the number of charge carriers created in the photoabsorption process combined with the tunnel noise (Goldie 1994), associated with the multiple tunnelling of charge carriers across the barrier, leads to an overall limiting resolution for a perfectly symmetrical junction of the form:

$$\mathrm{d}\lambda_T(nm) \sim 2.8\ 10^{-3}\lambda^{3/2}\Delta^{1/2}[F + 1 + (1/ < n >)]^{1/2}. \quad (2)$$

Here the Fano factor F can be assumed to be ~ 0.22, considered typical of many of the transition metal elemental superconductors such as tantalum (Rando et al. 1992). Thus for tantalum based STJ's the tunnel limiting resolution for the case when $< n > \rightarrow \infty$ is ~ 30 nm for $\lambda \sim 500$ nm.

At least two other components due to the readout noise of the analogue electronics ($\mathrm{d}\lambda_E$) and spatial non-uniformity's ($\mathrm{d}\lambda_S$),must also be added to a first approximation in quadrature,resulting in the measured resolution $\mathrm{d}\lambda_M(\lambda)$. The electronics component can be determined from the measured full width at half maximum ($\mathrm{d}Q_E$) of an average test charge $< Q_E >$ injected into the preamplifier with the STJ in circuit, such that $\mathrm{d}\lambda_E = \lambda(\mathrm{d}Q_E/ < Q_E >)$.

3. The tantalum STJ - experimental configuration

A number of workers have investigated devices which contain trapping layers, to enhance the multiple tunneling, for application at X-ray wavelengths (Gaidis et al. 1996; Mears et al. 1993; Poelaert et al. 1996). The results described here are for a tantalum based STJ whose geometry is illustrated in Fig. 1. The device consists of a 20×20 μm square 100 nm thick epitaxial tantalum film on a smooth sapphire substrate on top of which a 30 nm thick aluminium trapping layer is deposited. The insulating barrier, of order 1 nm thick, is formed through a controlled oxidation of this aluminium. The oxide barrier is capped by a further 30 nm aluminium trapping layer followed by a thin seed layer prior to the deposition of 100 nm of polycrystalline tantalum. The leads are 2 μm wide and made of niobium to prevent quasiparticle losses down the leads from the lower bandgap materials of tantalum and aluminium. Further details on these devices can be found in Verhoeve et al. (1996a), while the role of the aluminium trapping layers is discussed in Poelaert et al. (1996). The original theoretical concept of quasiparticle trapping is described by Booth (1987).

Prior to establishing the optical performance of the device the key electrical characteristics were derived through the investigation of the $I - V$ function at 0.3 K. The bandgap of the device at the barrier was determined to be $\lambda_{Barrier} \sim 0.5$ meV. This is lower than that for bulk tantalum $\lambda_{Ta} \sim 0.66$ meV due to the proximity effect induced by the aluminium trapping layers. The resistivity of the barrier was estimated to be $\sim 2.6\ 10^{-6}\ \Omega$ cm^2 while the leakage current was $\sim 50 - 100$ fA μm^{-2} at ~ 0.1 mV.

The optical experiments have been performed in a ^{3}He cryostat at a base temperature of ~ 0.3 K. As shown in Fig. 1, the device was illuminated through the sapphire substrate (back illuminated), via a fibre optic, by photons

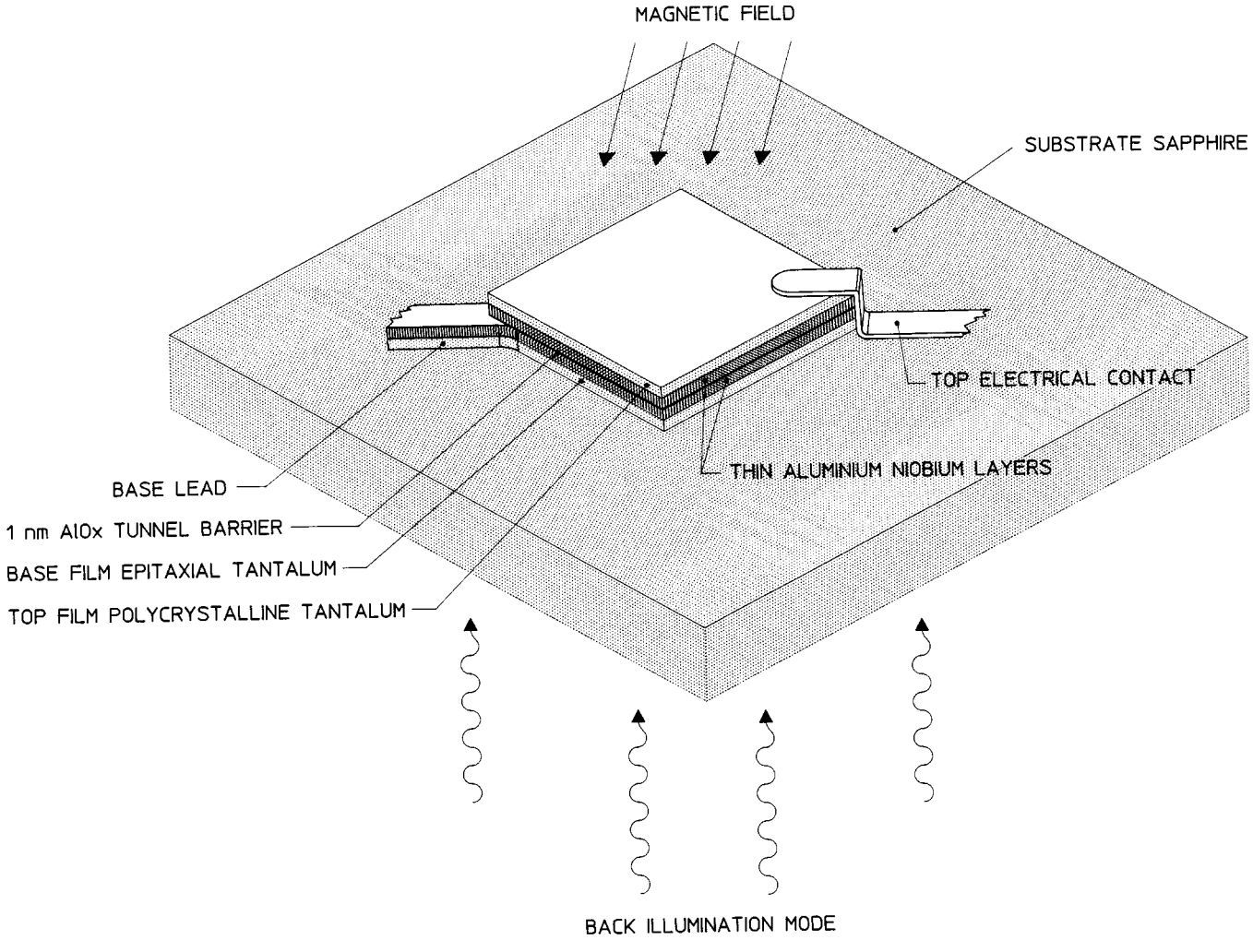

Fig. 1. A schematic of the tantalum tunnel junction used in the current experiments together with it's orientation in a parallel magnetic field so as to suppress the Josephson current. The device is operated in a back illuminated mode therefore the UV response is limited by the cut-off of the substrate

from a monochromatic xenon lamp light source. The illumination was initially at a very low intensity level ($\sim$ Hz) such that only a single optical photon was incident on the detector during the tunnel and electronics processing time. All optical illumination described here was in this back-illuminated mode. This mode is preferred for two reasons: i) all optical photons are absorbed in the high quality epitaxial tantalum film, the charge from which is trapped by the aluminium film close to the barrier. Note the top polycrystalline film will have a coating of tantalum oxides $\sim$ 5 nm thick (Peacock et al. 1997a) which may absorb a significant fraction of the optical photons if illumination was from the front. The resultant charge from photons absorbed in this oxide layer may well become trapped by such oxides. ii) The back illumination mode means that optical photons are not blocked by the lead to the top film. While this latter problem is minor for a single device, it would become a major issue when operating arrays where the number and layout of the top film connecting leads would cover a significant part of the top surface of the array.

The electrical signals from the STJ were read out using a charge sensitive amplifier operated at room temperature about 1 m from the device. Each detected optical photon gives rise to a pulse at the output of the preamplifier. The amplitude of this pulse is measured together with the pulse rise time and corresponds to the total number of tunnelled electrons (charge output) and signal decay time respectively. The electronic noise is continuously monitored through the response to an electronic pulse fed directly into the pre-amplifier. Typical noise values of $\mathrm{d}Q_{\mathrm{E}} \sim 3500$ electrons ($\mathrm{d}\lambda_{\mathrm{E}} \sim 28$ nm at ($\lambda \sim 500$ nm) were obtained. Here $\mathrm{d}Q$ represents the full width at half maximum (FWHM) of the typically gaussian shaped charge distribution. Further details of the

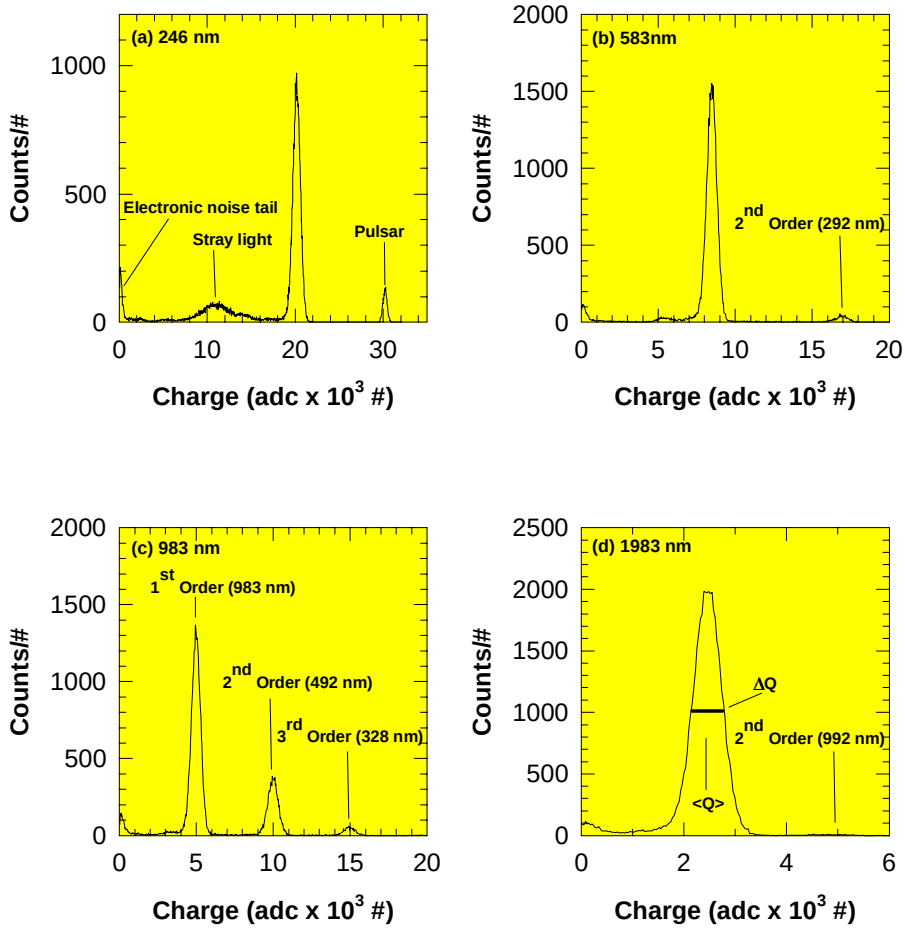

Fig. 2. The charge spectra obtained from the junction when illuminated with **a)** 246 nm , **b)** 583 nm, **c)** 983 nm and **d)** 1983 nm photons from a monochromatic light source. The charge is in units of ADC channel (#) as recorded by the signal pulse height analyser ($1\# = 6.24\ 10^3$ electrons)

experimental configuration can be found in Peacock et al. (1996, 1997a) and Verhoeve et al. (1997).

4. The detectors spectroscopic performance

Single photon pulses were measured at different wavelength setting of the monochromator from the UV (200 nm) to the near infra-red (2 μm). Sample spectra are shown in Fig. 2. The mean charge output $< Q >$ and the FWHM dQ provide a determination of the detector responsivity ($R_{\rm E}$) and measured spectral resolution $\mathrm{d}\lambda_{\rm M} \sim \lambda(\mathrm{d}Q/ < Q >)$ for a known photon wavelength. A typical responsivity of $R_{\rm E} \sim 2.5\ 10^4$ electrons/eV, equivalent to a mean number of tunnels for each charge carrier of $< n > \sim 30$, was derived. The peak at the end of the charge range in the spectrum of Fig. 2a is due to the pulsar used to determine the contribution to the measured resolution from the electronics $\mathrm{d}\lambda_{\rm E}$. At some wavelengths the second and third order from the monochromator are also apparent rather nicely illustrating the detectors intrinsic spectroscopic capability. The short and long wavelength limits of 200 nm and 2 μm are due to the fibre optic cut-off.

Figure 3 illustrates the measured resolution $\mathrm{d}\lambda_{\rm M}$ of the device as a function of wavelength together with the resolution $\mathrm{d}\lambda_{\rm C}$ after correction for the electronic noise ($\mathrm{d}\lambda_{\rm E}$), as determined from the constant charge input pulse, such that $\mathrm{d}\lambda_{\rm C}^2 = \mathrm{d}\lambda_{\rm M}^2 - \mathrm{d}\lambda_{\rm E}^2$. The limiting resolution of the device ($\mathrm{d}\lambda_{\rm T}$) is also shown in Fig. 3, based on Eq. (2) with $< n > \sim 30$ and a value of $\Delta \sim 0.66$, corresponding to that of bulk tantalum. The agreement between $\mathrm{d}\lambda_{\rm T}$ and $\mathrm{d}\lambda_{\rm C}$ is very good indeed, indicating that the detector resolution at these wavelengths is totally dominated by the tunnel noise with little contribution from spatial variations to the responsivity ($R_{\rm E}$) as observed at X-ray wavelengths (Verhoeve et al. 1996, 1997). In addition the signal to noise ratio is also shown in Fig. 3 (inset).This allows an estimate of the current long wavelength response beyond that actually measured of ~ 2 μm. Assuming a five sigma detection criterion above the noise the detector is

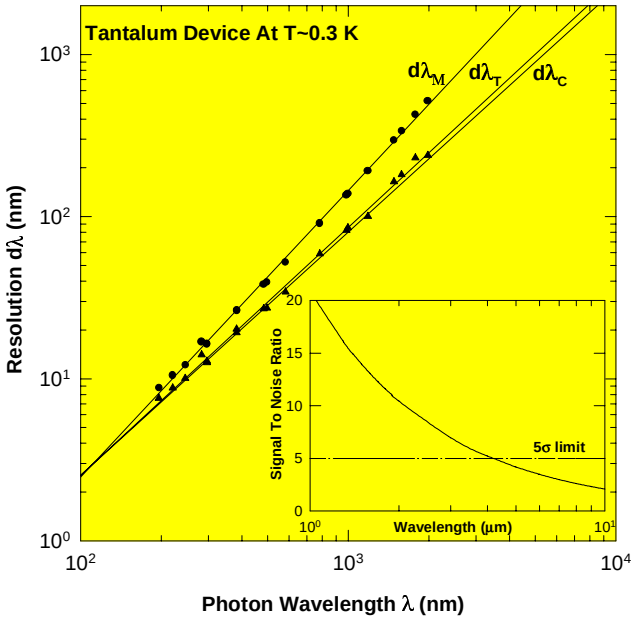

Fig. 3. The measured resolution ($d\lambda_M$) (•) and the electronics corrected resolution ($d\lambda_C$) (▲) as a function of wavelength together with the best linear fits. The theoretical variation with photon wavelength of the Fano plus tunnel noise limited resolution ($d\lambda_T$) based on Eq. (2) is also shown. The inset shows the current detectors signal to noise ratio (S/N) as a function of the near infrared photon wavelength in μm

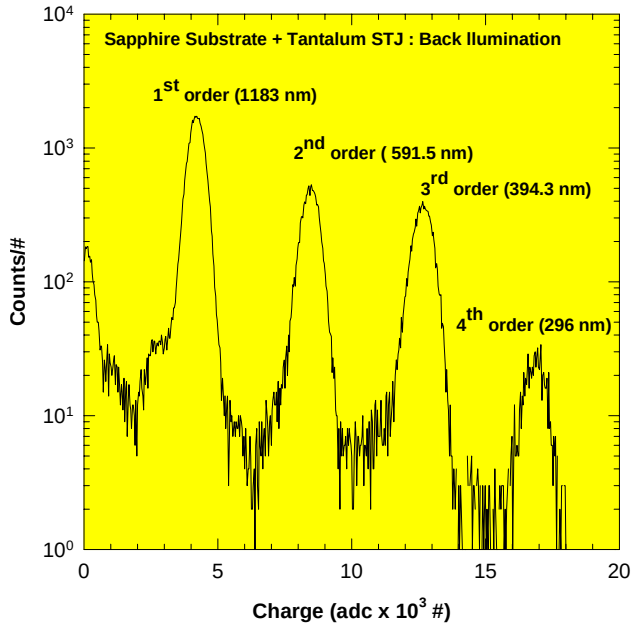

Fig. 4. The complete charge spectrum when the monochromator was set to select photons with a wavelength of 1183 nm. The grating orders 1 to 4 are all clearly resolved. Some distortion in the charge distribution at low and possibly higher charge levels can be discerned in each of these peaks and may be due to pile-up of events due to the signal process time of the electronics. Stray light and the incomplete conversion of the photons energy to charge carriers, due to possible substrate losses, have been ruled out as a major cause of such low intensity level tails in these spectra

currently limited by the electronic noise to wavelengths up to $\lambda_{max} \sim 4$ μm. Note this maximum wavelength (λ_{max}) can be simply written as $\lambda_{max}(\mu m) \sim [0.6\, R_E/dQ_E]$. Further reduction in the noise of the room temperature electronics would of course extend even further this value into the infrared.

The linearity of the detector with photon energy is best measured using the multiple orders from the grating. This removes effects such as response changes with drifting temperature or possible calibration errors since the output from the monochromator over several grating orders are exact multiples of the same wavelength. Figure 4 shows the charge spectrum from the device when illuminated with optical light via the grating monochromator, with such a grating response covering four orders from 1183 – 296 nm. Not only are the various orders well resolved but the charge output as a function of wavelength can be precisely determined. The linearity is very high with a maximum deviation from linearity with photon energy of below 0.6%.

5. The detector quantum efficiency

Theoretically the tantalum STJ has a remarkable efficiency to the absorption of photons ranging in wavelength from the ultraviolet to the near infrared. Currently an actual experimental measurement with a calibrated light source is experimentally not possible. Indirect methods can however be used to verify the theoretical data. Figure 5 (inset) illustrates schematically the principal sources of photon loss.

For $\lambda > 200$ nm the most significant factor effecting the detector quantum efficiency is the reflection of photons from the vacuum – sapphire (R_{Sap}) and sapphire-tantalum (R_{Ta}) interfaces in the back-illuminated mode. Figure 5 shows the total reflectivity resulting from reflections, including multiple reflections, at both these interfaces. These data are based on the optical constants for Sapphire and Tantalum from Palik (1985) and Weaver et al. (1981). Between $200 < \lambda < 700$ nm the reflectivity is always $< 50\%$. The reflectivity of the sapphire substrate as well as the substrate to tantalum interface can of-course be reduced through the use of anti-reflection coatings, albeit at the expense on bandwidth. The absorption (A_{Sap}) of the photon flux through the 0.5 mm thick R-plane sapphire is dramatic at short wavelengths ($\lambda < 200$ nm) while the reflectivity of the tantalum film (R_{Ta}) increases significantly at the long wavelengths ($\lambda > 600$ nm). These effects therefore limit the overall quantum efficiency of the device. It can be seen from Fig. 5 that the actual photon flux entering the thin

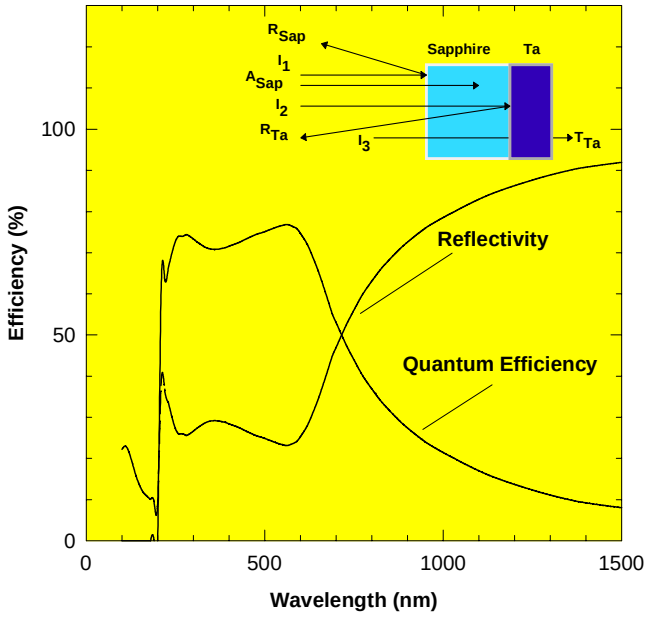

Fig. 5. The theoretical quantum efficiency and reflectivity for the current tantalum based STJ. The total reflectivity of both the vacuum-sapphire ($R_{\rm sap}$) and sapphire- tantalum ($R_{\rm Ta}$) interfaces are included in the overall reflectivity which includes multiple reflections, while in addition the attenuation in the sapphire ($A_{\rm sap}$) is included in the estimate of the quantum efficiency. The 92 nm thick base tantalum film transmits ($T_{\rm Ta}$) only $\sim 1\%$ at a peak wavelength of 600 nm of all photons not reflected at this interface. The inset illustrates the optical configuration where the quantum efficiency is simply defined as $1 - R_{\rm sap} - R_{\rm Ta} - A_{\rm sap} - T_{\rm Ta}$. Here the reflectivity and attenuation takes into account the case of multiple reflections between the sapphire and tantalum interfaces and the associated attenuation of the light in the sapphire

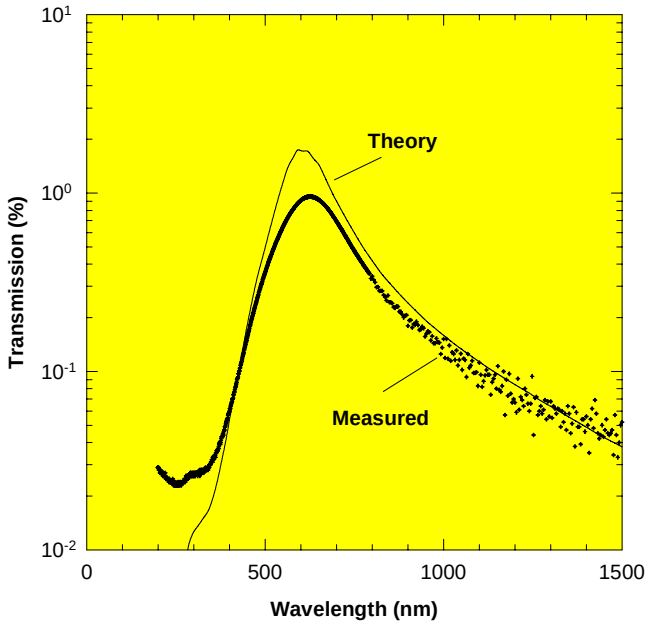

Fig. 6. The measured transmission (+) through a sample of 0.5 mm thick sapphire substrate coated with a 92 nm epitaxial tantalum film similar to the base film of the current STJ. For comparison the theoretical transmission for a 92 nm film deposited on a sapphire substrate is also shown

epitaxial tantalum film (thickness ~ 92 nm) is above 50% from $200 < \lambda < 700$ nm. Nearly all the photons entering the base epitaxial tantalum film will be absorbed. To demonstrate this the transmission through a 0.5 mm thick sapphire substrate covered by a 92 nm thick tantalum epitaxial film has been measured at 300 K and is shown in Fig. 6 together with the theoretical transmission based on the optical constants of Weaver et al. (1981). Some deviation exists probably due to the fact that the optical constants are derived for strain and oxide free bulk tantalum samples, while the experimental data is derived for an epitaxial thin film known to be coated with a few nanometers (~ 5 nm) of native tantalum oxide and sub-oxides. Even with this uncertainty the measured peak transmission is only $\sim 1\%$ at ~ 600 nm. Also this small number of photons is not totally lost but rather are absorbed in the top polycrystalline film of the STJ thereby still contributing to the overall response.

While a quantum efficiency predicted theoretically to be over 50% from $200 < \lambda < 700$ nm, peaking at $\sim 75\%$

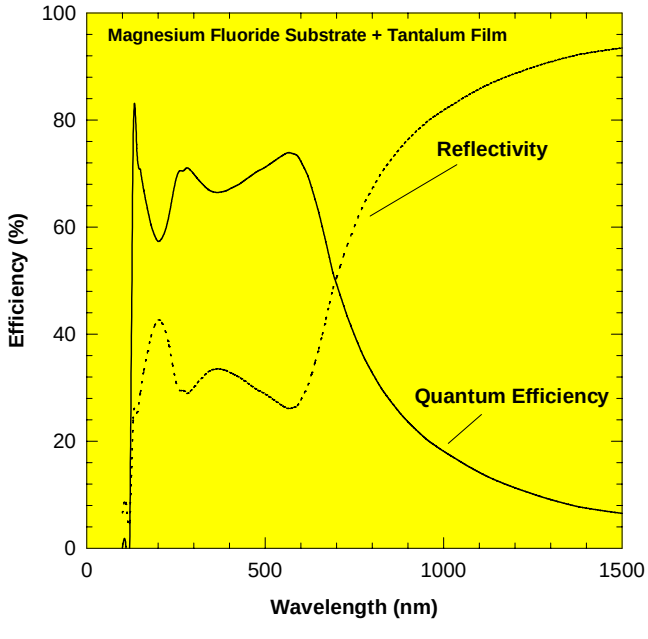

Fig. 7. The theoretical quantum efficiency and reflectivity for the current tantalum based STJ if deposited on a substrate of magnesium fluoride. The reflectivity of both the vacuum$-MgF_2$ and MgF_2 – tantalum interfaces are included in the overall reflectivity together with any multiple reflections, while in addition the overall attenuation in the MgF2 is included in the estimate of the quantum efficiency

at (peak $\sim$ 550 nm, is more than adequate for ground-based astronomical applications, the UV response is inadequate due to the cut-off of the sapphire substrate below $\sim$ 200 nm. An alternative for a space based telescope taking advantage of the UV response, would be to replace the sapphire substrate with one of magnesium fluoride. Figure 7 illustrates the system reflectivity (vacuum $-$ MgF_2 and MgF_2 $-$ Tantalum including multiple reflections) together with the predicted quantum efficiency assuming a 0.5 mm thick MgF_2 substrate. The short wavelength response has now been extended down to the cut-off of the MgF_2 ($\sim$ 110 nm) while the long wavelength optical response is largely unchanged. As yet no devices have been fabricated on MgF_2 although initial depositions of epitaxial tantalum films have been successful.

Any application of a superconducting tunnel junction for optical astronomy must also consider the effect of infrared background radiation. For wavelengths greater than a few microns the infrared flux from room temperature components could be considerable. These photons can still break Cooper pairs effectively increasing the thermal current in the device. This is equivalent to raising the operating temperature of the device. Naturally this flux can be reduced in any practical application through careful optical design. The current device does however have a significant intrinsic infrared rejection capability through the reflection properties of the sapphire and tantalum. Figure 8 illustrates the measured reflectivity [$R_{\rm M}$] of a sample (sapphire $\sim$ 0.5 mm thick plus a 92 nm thick tantalum film) at 300 K as a function of wavelength. The theoretical reflectivity [$R_{\rm T}$] is also shown highlighting the decreased reflectivity between 5 and 12 μm, although this is also accompanied by an increased absorption. The measured reflectivity [$R_{\rm M}$] also shows such a window which, although it reaches close to 100% for $\lambda > 14$ μm, is significantly lower than calculated at $\lambda < 5$ μm ($R_{\rm T} \sim 95\%$ and $R_{\rm M} \sim 50\%$). For comparison the normalised photon flux from a blackbody at 20 C is also shown [BB(20C)]. The total efficiency [$E_{\rm T}$] to infrared photon detection is also shown in Fig. 8. This efficiency contains the reflection from both the sapphire and tantalum interfaces (including multiple reflections) as well as absorption in the sapphire. Convolving the overall IR rejection efficiency with the 20 C blackbody photon spectrum between $1-100$ μm indicates that $< 0.1\%$ of this blackbody radiation will enter the tantalum STJ. The situation is however not quite so favourable for MgF_2 substrates.

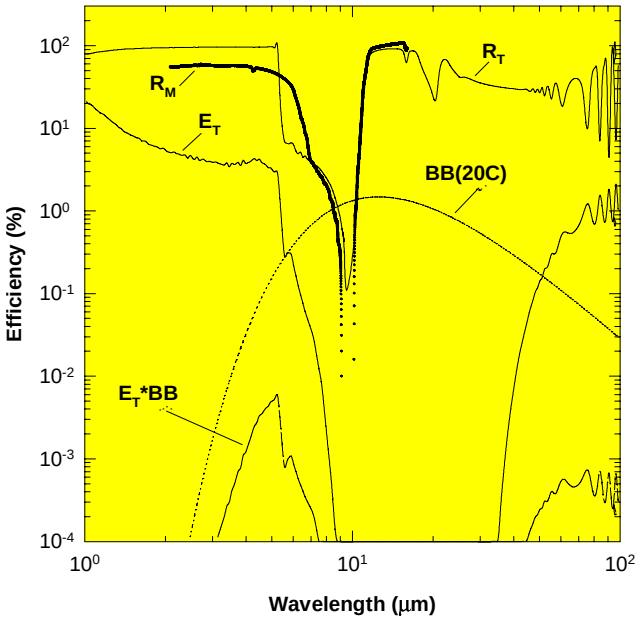

Fig. 8. The infrared reflectivity $R_{\rm M}$ (+) as measured with an IR reflectometer of a representative sapphire plus 92 nm tantalum film as a function of wavelength. For illustrative purposes the photon flux from a blackbody at 20 C [BB(20C)] normalised such that the photon number spectral integral equals one is also shown, together with the theoretical reflectivity $R_{\rm T}$ and overall infrared detection efficiency [$E_{\rm T}$]. The convolution of the rejection efficiency $E_{\rm T}$ with the photon flux from the blackbody [BB(20C)] is also shown [$E_{\rm T}$*BB]

6. Conclusion

In conclusion we have shown that a tantalum superconducting tunnel junction should have considerable potential as a photon counting broad band low resolution spectrometer in optical and ultraviolet astronomy. Already the spectroscopic resolution has nearly reached the theoretical limit for symmetrical tunnel junctions, of below 10 nm at wavelengths shorter than $\sim$ 250 nm. The key features can therefore be summarised as follows:

a) Photon counting with an inherent spectroscopic capability from the ultraviolet ($\sim$ 200 nm) to the near infrared ($\sim$ 2 μm) with d$\lambda_{\rm M} \sim$ 50 nm at 550 nm. Simple signal to noise calculations show that single photon detection is still possible up to wavelengths of order $\lambda_{\rm max} \sim 4$ μm.

b) A theoretical quantum efficiency ranging from $60-20\%$ over the waveband 200 nm to 1.0 μm respectively peaking at $\sim 75\%$ for $\lambda_{\rm max} \sim$ 550 nm. It should also be possible to extend the short wavelength limit to 110 nm through the replacement of the sapphire substrate with magnesium fluoride.

Future developments must involve the practical astronomical application of such devices through the development of arrays. The first of these have already been fabricated and are already under evaluation (Jansen et al. 1996).

Acknowledgements. The authors acknowledge the technical support of A. van Dordrecht (ESTEC), R .Venn of Cambridge Microfab Ltd. UK and D. Goldie of Oxford Instruments Ltd. UK. The many fruitful discussions with M.A.C. Perryman, and P. Jakobsen of the Space Science Department ESA on the potential applications of such detectors are gratefully acknowledged.

References

Booth N.E., 1987, Appl. Phys. Lett. 50, 293
Fano U., 1947, Phys. Rev. 72, 26
Gaidis M.C., Friedrich S., Segall K., et al., 1996, IEEE Trans. Applied Superconductivity 6, 1
Goldie D.J., Brink P. L., Patel C., Booth N.E., Salmon G.L., 1994, Appl. Phys. Lett. 64, 3169
Gray K., 1978, Appl. Phys. Lett. 32, 392
Jansen F.A., Peacock A., Rando N., et al., 1996, SPIE 2808, 516
Mears C.A., Labov S.E., Barfknecht A.T., 1993, J. Low Temp. Phys. 93, 561
Palik E.D., 1985, Handbook of optical constants of solids. Academic Press Inc
Peacock A., Verhoeve P., Rando N., et al., 1996, Nat 381, 135
Peacock A., Verhoeve P., Rando N., et al., 1997a, J. Appl. Phys. 81, 11, 7641
Peacock A., Verhoeve P., Rando N., et al., 1997b, A&AS 123, 581
Perryman M.A.C., Foden C.L., Peacock A., 1993, Nucl. Instr. Meth. A325, 319
Poelaert A., Verhoeve P., Rando N., et al., 1996, SPIE 2808, 523
Rando N., Peacock A., van Dordrecht A., et al., 1992, Nucl. Instr. Meth. A313, 173
Verhoeve P., Rando N., Peacock A., et al., 1997, IEEE Trans. App. Superconductivity 7, 3359
Verhoeve P., Rando N., Verveer J., et al., 1996, Phys. Rev. B. 53, 809
Weaver J.H., Krafka C., Lynch D.W., Koch E.E., 1981, Physik Daten, 18-1
Wood G.H., White B., 1969, Appl. Phys. Lett. 15, 237